DOI: 10.13009/EUCASS2023-318
Aerospace Europe Conference 2023 – 10TH EUCASS – 9TH CEAS

Investigating the influence of turbofan engine design on climate for a short-to-medium-range flight network

Harjot Singh Saluja [⋆†], *Feijia Yin and Arvind Gangoli Rao*[⋆]
[⋆] *Delft University of Technology*
Faculty of Aerospace Engineering, Kluyverweg 1, 2629HS, Delft
h.s.saluja@tudelft.nl · f.yin@tudelft.nl · a.gangolirao@tudelft.nl
[†]Corresponding author

Abstract

The climate impact of aviation is mainly due to the emission of species such as CO_2, water vapour, NO_x, and contrails. The non-CO_2 effects contribute more significantly than CO_2 warming, particularly NO_x and contrails. This research analyzes the impact of changing turbofan engine design on the climate, taking into account the major non-CO_2 effects. The climate impact of the emissions due to the conventional kerosene-based Jet A-1 as well as that due to the lifecycle emissions of one of the CORSIA-eligible SAFs is analyzed. A detailed methodology consisting of aircraft/engine performance estimation, emission prediction, and climate impact evaluation is implemented for a subset of the global A320 flight network. The tradeoff between different species' responses and the fuel consumption change is analyzed. It was found that for the considered fleet and growth trend, contrails contribute the largest towards the total climate response, and thus, are the driving factor of the total response change. The implementation of SAF reduces CO_2 and contrail-related climate effects significantly, enabling engines with higher pressure ratios to have an improved climate response than the conventional Jet A-1 fuel-driven designs.

1. Introduction

Aviation is one of the key pillars on which the modern society stands. It enables knowledge, technical and cultural exchange at an unprecedented level compared to the past. The demand for aviation has steadily increased over time with momentary setbacks induced due to global events such as the oil crisis of the 70s or the financial crisis during 2008-09.[a] Thus, based on the past trends, it is expected that despite the global COVID-19 pandemic, the sector will continue to experience growth, particularly in rapidly growing economies. With increase in demands comes the challenge of reducing the climate impact of aviation. According to IPCC,[1] the current contribution of aviation to the total anthropogenic effective radiative forcing (ERF) is about 3.5%. This is set to rise in the future due to demand forecasts as well as the decarbonization of other sectors. The CORSIA, introduced by ICAO focuses on offseting the CO_2 emissions to enable net-zero growth of aviation.[2] One key element of this initiative is the development and implementation of sustainable aviation fuels (SAF). On a lifecycle scale, these fuels have a net lower carbon footprint than the conventional kerosene-based Jet A-1. However, to meet ambitious climate goals, the non-CO_2 emissions from aviation need to be taken into account. These emissions, particularly the effects of NO_x and contrails, contribute close to 66% of the total aviation ERF.[2] There needs to be a rapid adaptation of climate-friendly technological advancements in the field of aircraft propulsion to tackle the non-CO_2 effects. In the past, the goal of civil turbofan engine design has been to optimize the engine for low fuel consumption and operating costs. While this has the benefit of reduced CO_2 emissions, a key greenhouse gas (GHG), the non-CO_2 emissions, particularly NO_x and non-volatile particulate matter (nvPM), i.e. soot emissions, increase. In addition, the formation of contrails also increases due to higher engine efficiencies[3,4] as well as soot particles acting as precursors for contrail ice particles.[5]
Within this context, in this research, the climate impact of aviation emissions is analyzed w.r.t. improvements in the engine design, along with the effect of introducing SAF, produced via the Hydroprocessed Esters and Fatty Acids (HEFA) Fuel Conversion Process, with soy being the feedstock. The baseline engine and aircraft combination chosen are the CFM56-5B4/P and the Airbus A320 respectively. A constant cruise altitude and Mach no. were considered. The operating pressure ratio (OPR) and the bypass ratio (BPR) of the engine are increased to analyze the tradeoff between improved fuel consumption and the total climate effect. With this objective in mind, in-house aircraft performance,

[a]https://www.icao.int/Newsroom/Pages/2021-global-air-passenger-totals-show-improvement.aspx

DOI: 10.13009/EUCASS2023-318

semi-empirical NO_x emission and nvPM emission models have been developed which combined with an engine model of the CFM56 in the Gas Turbine Simulation Program (GSP)[6] are used to generate the overall aircraft performance profile in terms of fuel consumption and key emissions. This is combined with a subset of the global A320 fleet to generate an emission inventory, which is used in the state-of-the-art climate impact assessment tool, AirClim[7,8] as an input to compute the Average Temperature Response for a time horizon of 100 years (ATR_{100}), the chosen climate response metric. For each variation in a design parameter of the engine, a corresponding emission inventory is generated and the ATR_{100} is evaluated, for identical background conditions in AirClim. This enables the comparison of the ATR_{100} with the fleet fuel consumption as a function of the engine design parameters.
In the next few sections, the models have been briefly described, followed by the main findings of the research, leading to the relevant discussion and conclusions.

2. Models and Methodology

2.1 Aircraft Performance

For an aircraft cruising at a constant altitude and Mach no., the aircraft weight changes continuously due to fuel burn. To maintain a constant Mach no., the aircraft thrust reduces over time during cruise. In this research, the average thrust during the cruise phase ($F_{avg.aircraft}$) was considered, calculated as:

$$F_{avg.aircraft} = \frac{W_{avg.} \cdot g}{\left(\frac{L}{D}\right)} \tag{1}$$

with $W_{avg.}$ as the mean of the aircraft weight at the beginning of the cruise, W_{start} and the end of the cruise, W_{end}. W_{start} consists of the Operating Empty Weight (OEW), cruise fuel weight ($W_{f,cruise}$), and the *apparent* payload weight $W_{app.payload}$, consisting of the actual payload weight, the fuel weights for descent and approach phases of the flight, and the reserve fuel weight. W_{end} is simply the difference between W_{start} and $W_{f,cruise}$, and L/D is the lift-to-drag ratio. With $F_{avg.aircraft}$ known, the cruise time (t_{cruise}) was calculated as:

$$t_{cruise} = \frac{W_{f,cruise}}{TSFC.F_{avg.aircraft}} \tag{2}$$

where TSFC is the thrust-specific fuel consumption during cruise. With the cruise time known at a particular Mach no., the cruise distance, d_{cruise} could be calculated. For this research, a constant cruise altitude of 33000 ft and Mach no. of 0.78 were assumed, with the payload consisting of 150 passengers at 90 kg each including baggage. This approach was tested with results from PIANO-X,[b] a widely-used aircraft performance tool, for a few test cases. For the design range and standard payload for a number of different aircraft (the A300, A340, B767 and the A320 and A320neo) at a constant cruise altitude and Mach no., it was found that the model predicted the thrust requirements, the cruise time and cruise distance within ± 2.5% w.r.t.. PIANO-X for a known cruise fuel weight.

2.2 Engine Performance: Gas Turbine Simulation Program (GSP)

The aircraft performance model described in the previous section is closely integrated with the engine model. While the former provides the thrust as an input for the engine, the latter provides the thrust-specific fuel consumption (TSFC) back to the performance model for determining the t_{cruise}. In addition, the engine model also provides the relevant thermodynamic parameters as well as the fuel flow to the in-house emission models and the emission inventory model respectively, described in the subsequent sections. Thus, the engine model serves as the core of the methodology needed to create the relevant inputs for subsequent climate assessment. GSP, which was used for the purpose of engine modelling, allows for individual variations of engine design parameters, making it suitable for this research. Within GSP, a "design point" needs to be defined based on which other "off-design" conditions can be simulated. Essentially, the design point is a reference condition, and based on the principles of mass, momentum and energy conservation, other off-design conditions can be generated from this design point.[9] In this research, the rated thrust setting at static sea-level (SLS) conditions was taken as the design point, whereas cruise was taken as the off-design condition. The engine parameter data for the baseline engine configuration was taken from the ICAO databank[c] (ICAO UID: 3CM026). This engine has an OPR of 27.69 and a BPR of 5.9, for a rated thrust of 120.11 kN. It is to be noted that the design point does not refer to the condition for which a turbofan engine is designed and optimized based on the top-level aircraft

[b] https://www.lissys.uk/piano-x-guide.pdf
[c] https://www.easa.europa.eu/en/domains/environment/icao-aircraft-engine-emissions-databank

DOI: 10.13009/EUCASS2023-318

and/or engine requirements, rather, in the context of this research, it only means as a reference operating condition, where the engine parameters and its performance is known beforehand.

2.3 NO_x emission model

To estimate the cruise NO_x emissions, the $P_3 - T_3$ method is implemented, given in Equation 3.

$$EINO_{x,cruise} = EINO_{x,SLS} \cdot \left(\frac{P_{t3,cruise}}{P_{t3,SLS}}\right)^n \cdot \left(\frac{FAR_{cruise}}{FAR_{SLS}}\right)^m \cdot exp(H) \tag{3}$$

where $EINO_x$ is the emission index of NO_x emissions, the ratio of the mass of NO_x emissions, and the fuel consumption, in grams/kg of fuel. In this method, the cruise NO_x emission index ($EINO_{x,cruise}$) is obtained by applying corrections to the $EINO_x$ at a reference condition ($EINO_{x,SLS}$), due to changes in the combustor inlet pressure (P_{t3}), fuel-to-air ratio (FAR) and humidity at cruise compared to the reference condition for similar combustor inlet temperature (T_{t3}). While the $EINO_{x,SLS}$ for most of the well-known turbofan engines is known from the ICAO databank, for this research, the variation of design parameters resulted in engine configurations that are not present in the databank. Therefore, a separate NO_x emission model was developed as a function of combustor inlet properties, P_{t3} and T_{t3} as well as FAR, inputs from GSP. Three CFM56 models available in the ICAO databank, having similar combustor technology levels as the baseline CFM56, were simulated in GSP for the landing-and-takeoff (LTO) cycle,[d] and the resulting parameters were curve-fitted to obtain the $EINO_{x,SLS}$ correlation, shown in Equation 4.

$$EINO_{x,SLS} = 0.1921 \cdot P_{t3}^{-0.7686} \cdot e^{0.0084 \cdot T_{t3}} \cdot 2.01^{60 \cdot FAR} \tag{4}$$

This correlation was tested with two other CFM56 models for the LTO cycle, and was found to predict $EINO_x$ within ± 10% of the ICAO $EINO_x$ values. For $EINO_{x,cruise}$ in Equation 3, the values of n and m were taken to be 0.3 and 0 respectively,[10] with the humidity correction term found to be approximately 1.1265, as suggested by the ICAO Annex 16 for 60% relative humidity at 33000 ft.[11]

2.4 The nvPM model

nvPM plays a key role in the formation of contrails, as the particles activate to form ice nuclei, further forming ice crystals under favorable conditions. In one of the experimental campaigns by the Deutsches Zentrum für Luft- und Raumfahrt (DLR) and the National Aeronautics and Space Administration (NASA), it was observed that the activation rate from soot particles to ice crystals for an A320 at typical cruise altitudes is significantly high, i.e. around 80-100%.[5] To quantify the resulting changes in contrail RF due to changes in contrail properties, as the nvPM emissions vary across engine configurations, the correlation from Grewe et al. (2021)[12] is implemented, which is as follows:

$$\Delta RF^{contr.} = \frac{arctan(1.9 \Delta pn^{0.74})}{arctan(1.9)} \tag{5}$$

where $\Delta RF^{contr.}$ is the contrail radiative forcing changes and Δpn refers to the change in nvPM number emissions relative to the nvPM number emissions of the baseline configuration. This correlation is only valid for $\Delta pn \geq 0.1$, as the condensation of heavier volatile particles (e.g. sulphates) starts to play a role in contrail ice crystal formation at very low nvPM numbers.

The dependency of nvPM on engine operating conditions is modeled based on the methodology given by Durdina et al. (2017).[13] The nvPM mass emission index at cruise conditions ($EI_{m,cruise}$) is obtained by applying pressure and FAR corrections to the reference EI ($EI_{m,SLS}$) for the same operating T_{t3}. To obtain the nvPM number emission index ($EI_{num,cruise}$), a parameter ν is used, which is the ratio of EI_{num} and EI_m. ν is found to be a function of T_{t3} and independent of the changes in altitude.[13] The ($EI_{m,SLS}$) and ν were modelled as a function of T_{t3} using data from the most recent version of the ICAO databank, which gives the nvPM indices for the LTO cycle for different engines. Six different CFM56 configurations were simulated in GSP for the LTO cycle, and the $EI_{m,SLS}$ and ν were curve-fitted as a function of the resulting T_{t3} from the simulations. The resulting correlations were tested at SLS conditions with two other CFM56 configurations, and at cruise conditions with a test case (a Boeing 737NG equipped with a CFM56-7B) given in the original research.[13] The model was found to predict the SLS EI values within ± 4% of the LTO cycle values, and the $EI_{m,cruise}$ and $EI_{num,cruise}$ within ± 10% and ± 6% respectively.

[d] https://www.easa.europa.eu/en/domains/environment/icao-aircraft-engine-emissions-databank

DOI: 10.13009/EUCASS2023-318

2.5 Emission inventory model

An emission inventory generally contains information about the location, the fuel burn, the emissions, and their frequency over a period of time. For this research, a subset of the 2019 global A320 network was downselected.[e] The objective was to select the busiest routes (annual total number of flights) while keeping the representation of the region-wise traffic of the A320 network in consideration, shown in Figure 1. Flights less than 500 km of total distance were not

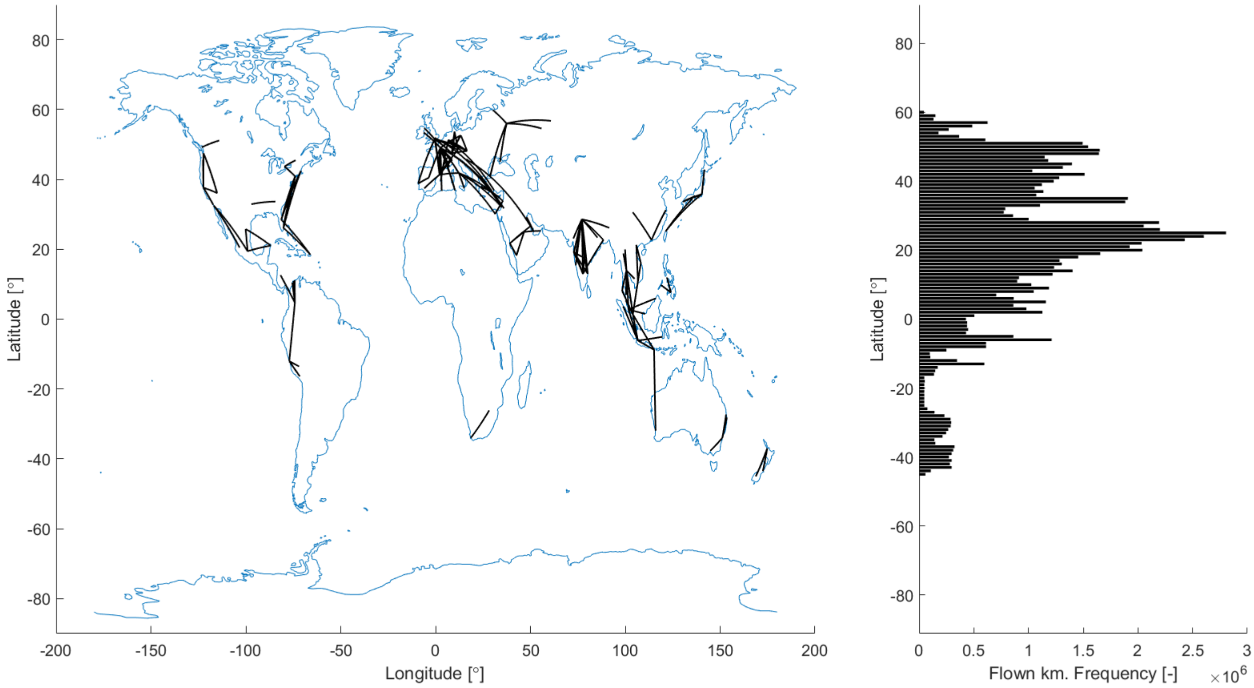

Figure 1: Flight network of the A320 aircraft considered in this research.

considered. Back-and-forth flights between a city pair were considered equal. Out of a total of 13868 city pairs where A320 flights were operational, 146 were selected, approximately 1.05%. Based on the selected criteria, the network represents 18.08% of the global 4.49 million A320 flights and 13.09% of the global 6.43 billion A320-flown km in 2019. The latitude distribution of the global flown kilometers is shown on the right, highlighting a large number of flights in the mid-to-high latitudes region. The position data (latitude and longitude) for each city pair was obtained at an interval of 10 km, resulting in a series of positional waypoints. For each city pair, first, the great circle distance was obtained. Combined with a constant cruise altitude and Mach no., the thrust requirements were determined from the aircraft performance model as described in section 2.1. Further, these conditions were simulated in GSP to obtain the thermodynamic cycle parameters of the engine performance, enabling cruise NO_x and nvPM calculations. Combined with fuel consumption, these parameters were then attributed to each waypoint, thus resulting in fuel and emission information at each waypoint. Finally, all the waypoints of all the city pairs were combined and arranged in a suitable format to form a single emission inventory.

2.6 Climate response model: AirClim

AirClim is a state-of-the-art climate assessment model that is designed to compare aviation technological options.[7,8] The key advantage of AirClim is that it uses linearized response functions to determine the response at geographical locations based on pre-calculated responses obtained from complex climate-chemistry models (CCMs). This reduces the computational time drastically, allowing for quick comparisons of different scenarios and cases. To estimate the climate response, two inputs are needed, a background scenario which is combined with the emission inventory (described in Section 2.5). The background scenario indicates the growth of the chosen fleet. In this research, the *CurTec* scenario was taken as the background. This scenario does not consider the general improvement in aircraft efficiency

[e] https://www.flightradar24.com/

DOI: 10.13009/EUCASS2023-318

over time due to technological progress, thus considering only the traffic growth due to demand. The growth trend was obtained from Grewe et al. (2021).[12] The background atmospheric CO_2 and CH_4 trends also need to be defined, as the response of these species depends on the background atmospheric concentrations. These trends were obtained from IPCC Shared SocioEconomic Pathways (SSPs).[14] Specifically, the SSP2-4.5 pathways were considered for the development of both species. The climate simulations start in 2015 and end in 2150. Further, a year needs to be defined when the emission inventory is representative of the background aviation scenario. This leads to a normalization of the background scenario based on the total fuel consumption of the emission inventory. This year was taken to be 2019, the same year for which the traffic was downselected. This was also the year from which the ATR_{100} is measured. The climate response was obtained for six key species: CO_2, H_2O, CH_4, O_3, contrails, and primary-mode ozone (PMO). The responses of CH_4, O_3, and PMO were combined as the overall NO_x emissions response, as the complex chemistry involving these species results in both warming (due to tropospheric O_3 enhancement) and cooling effects (due to CH_4 depletion, and consequently, lowered O_3 enhancement), but overall a warming effect.[2,15]

2.7 Climate sensitivity of engine design

2.7.1 Engine design space

The design parameters were varied in GSP for the baseline CFM56-5B4/P engine at the design point (SLS-takeoff condition), resulting in different combinations of design parameters, constituting a matrix of engine configurations. Three BPRs were considered, i.e. BPR = 5, BPR = 6, and BPR = 7. First, for each BPR, the optimum Fan Pressure Ratio (FPR) was obtained, i.e. the BPR-FPR combination with the lowest TSFC at the design point. Then, for each BPR-FPR combination, the OPR was varied from 25 to 40 in steps of 5. For each of these OPRs, the Turbine Inlet Temperature (TIT) was varied to determine the combination with the lowest TSFC at the design point. Thus corresponding to each BPR, there were four engines modelled, one at each OPR. In total, 12 configurations were modelled in GSP, and for each of these configurations, a corresponding emission inventory was generated. In addition, the total nvPM particle number for the whole fleet was calculated for each configuration and the difference with the baseline configuration was used as the input to Equation 5 to obtain the relative difference in contrail RF between the baseline and the corresponding configuration. Together, these serve as the inputs to AirClim, for the same background settings (*CurTec* as the background scenario with SSP2-4.5 pathways for the background atmospheric CO_2 and CH_4).[14]

2.7.2 Life Cycle Assessment (LCA) of SAF implementation

Depending on the feedstock used in production and the pathway of production, different SAFs have different life-cycle emissions, expressed in terms of equivalent CO_2 emissions (in grams) per megajoules (gCO2e/MJ). The life-cycle emissions for SAFs consist of two elements: the core life-cycle emissions and the induced land-use change (ILUC) emissions. For the chosen HEFA pathway and soy feedstock, the global-averaged core life-cycle emissions are 40.4 gCO2e/MJ and the ILUC emissions are 25.8 gCO2e/MJ, the total being 66.2 gCO2e/MJ. Considering similar LHV as Jet A1 at 43 MJ/kg fuel, the equivalent life-cycle $EICO_2$ is 2.85 kg CO_2/kg fuel, i.e. 9.71% lower than that of Jet A-1, which is 3.15 kg CO_2/kg fuel. In addition to life-cycle CO_2 emissions, SAF also have lower nvPM $EI_{num.}$, due to differences in the fuel hydrogen content. In the previously mentioned experimental campaign,[5] there were different blends of kerosene and SAF HEFA tested, and the particle number emissions, as well as their tendency to form ice nuclei, were analyzed. It was observed that the nvPM $EI_{num.}$ were ≈ 45-53% lower than the reference Jet A-1 fuel.[5] In this research, a reduction of 50% in nvPM $EI_{num.}$ from SAF was considered, along with lower and upper-limits of 45% and 53% respectively, to analyze the sensitivity of the climate response w.r.t.. these changes.

3. Results

First, the results of the baseline engine are discussed. These include the fuel and emissions, as well as the individual climate response of each species. The results for the baseline engine serve as the reference condition with which results for other configurations, as well as those for the SAF implementation, are normalized and compared. Next, the variation of the climate metric ATR_{100} w.r.t. the fleet fuel consumption is analyzed as a function of the changes in the engine design parameters.

3.1 Baseline engine performance

The baseline CFM56-5B4/P performance is reported in Table 1. Over one year, the average fleet-level $EINO_x$ at cruise is 11 g/kg fuel, and the averaged fleet-level nvPM $EI_{num.cruise}$ is $4.85 * 10^{14}$. The ATR_{100}, measured from 2019 and

DOI: 10.13009/EUCASS2023-318

averaged over 100 years is 1.57 milli-kelvins [mK].

Table 1: Performance parameters for the baseline CFM56 engine. These are annual fleet-level results.

	Fuel Consumption [Tg]	**NO_x emissions [Tg]**	**nvPM no. 10e24 [#]**	**ATR_{100} [mK]**
Baseline CFM56-5B4/P	2.28	0.025	1.1	1.57

Table 2: The contribution of climate-relevant species towards the total temperature response.

Species [-]	**CO_2**	**H_2O**	**Contrails**	**NO_x**
$ATR_{100,spec}$ [mK]	0.20	0.018	1.05	0.30
(%)	(12.81%)	(1.13%)	(67.13%)	(18.93%)

It is important to identify the contribution of the relevant species' (given in Section 2.6) temperature response to the total temperature response for the baseline configuration. Table 2 shows the contribution of these species toward the total response. The contribution of contrails is greater than two-thirds. There are two reasons for the same. First, the aircraft is assumed to be flying at a constant altitude. This implies that a large portion of the traffic of the selected fleet is in the mid-to-high latitude region, where the ice-supersaturated regions (ISSR) occur around the chosen altitude. Also, none of the fuel consumption at lower altitudes during the LTO cycle and the climb phase is considered. These altitudes do not have favorable conditions for contrail formation. Secondly, the fleet does not consist of any other aircraft. This leads to all of the ISSR in a local region being available for the chosen aircraft. Together with NO_x and H_2O, the contribution of the non-CO_2 responses is greater than 85%.

3.2 ATR_{100} v/s fleet fuel consumption

With the baseline results established, the results of the other engine configurations of the design space are explored. Specifically, the variation of the climate metric ATR_{100} w.r.t. the fleet fuel consumption is analyzed for the changing engine configuration at design point. This is shown in Figure 2. As expected, increasing the OPR and BPR reduces the fuel consumption due to increased cycle efficiency, but the corresponding total ATR_{100} increases as well. On average, across the different BPRs, the increase in the pressure ratio from 25 to 40 reduces fuel consumption by 4.3%. On the other hand, the increase in the ATR_{100} is more sensitive. For BPR = 5, the increase in the ATR_{100} is close to 46% between OPR = 25 and OPR = 40, which reduces to 38% at BPR = 7. The implementation of SAF is more non-linear, as it affects both CO_2 as well as a key non-CO_2 species, i.e. contrails. Relative to the corresponding Jet A-1 case, the greatest reduction in the climate impact was found to be 19.93%, at the OPR = 25, BPR = 5 engine configuration, while the smallest was found to be 7.8%, at the OPR = 40, BPR = 7 configuration. The reduction potential of climate impact due to the implementation of SAF reduces with increasing OPR and BPR, although OPR, keeping the range of variation in consideration, is found to be the more sensitive parameter. This large range of the reduction potential is due to the effect on contrails ATR_{100}, which is the largest contributor, as seen from Table 2. Instead of 50%, if a larger reduction of 53% in the nvPM $EI_{num.}$ is considered, the corresponding decrease in the total ATR_{100}, compared to the Jet A-1 configuration, is approximately 1-2% more. On the other hand, a lower reduction of 45% in the nvPM $EI_{num.}$ causes an increase in the corresponding ATR_{100}, ranging from 2.2% to 3.4%. In line with previous observations, smaller changes compared to the Jet A-1 configurations, occur at the high-OPR, high-BPR configurations, and vice-versa.

Irrespective of the type of fuel, one of the key observations from Figure 2 is that the change in the fuel consumption and the total ATR_{100} is not the same for a particular variation in engine design. For instance, if the two extreme configurations at the lower right (OPR = 25, BPR = 5) and the upper left (OPR = 40, BPR = 7) of the figure are considered for the Jet A-1 fuel, the reduction in the fuel consumption is 9.02%, while the increase in the total ATR_{100} is 47.36%, close to five times the fuel consumption decrease. This large increase in the ATR_{100} is mainly due to the larger non-CO_2 effects of NO_x and contrails as the pressure ratio and bypass ratio increase. While the individual contributions of the key non-CO_2 responses, which form a large component of the total response, are highlighted in Table 2, it is important to analyze the impact of changing engine design on these contributions. This is highlighted in Figure 3, where the individual species' response change corresponding to their baseline values are shown for increasing OPR at BPR = 5. The response changes for CO_2, NO_x, and contrails are shown, along with the total response. The H_2O effects are not shown, as these have a negligible contribution towards total climate impact. A positive change implies that the effect is increasing w.r.t. baseline configuration, and vice-versa.

DOI: 10.13009/EUCASS2023-318

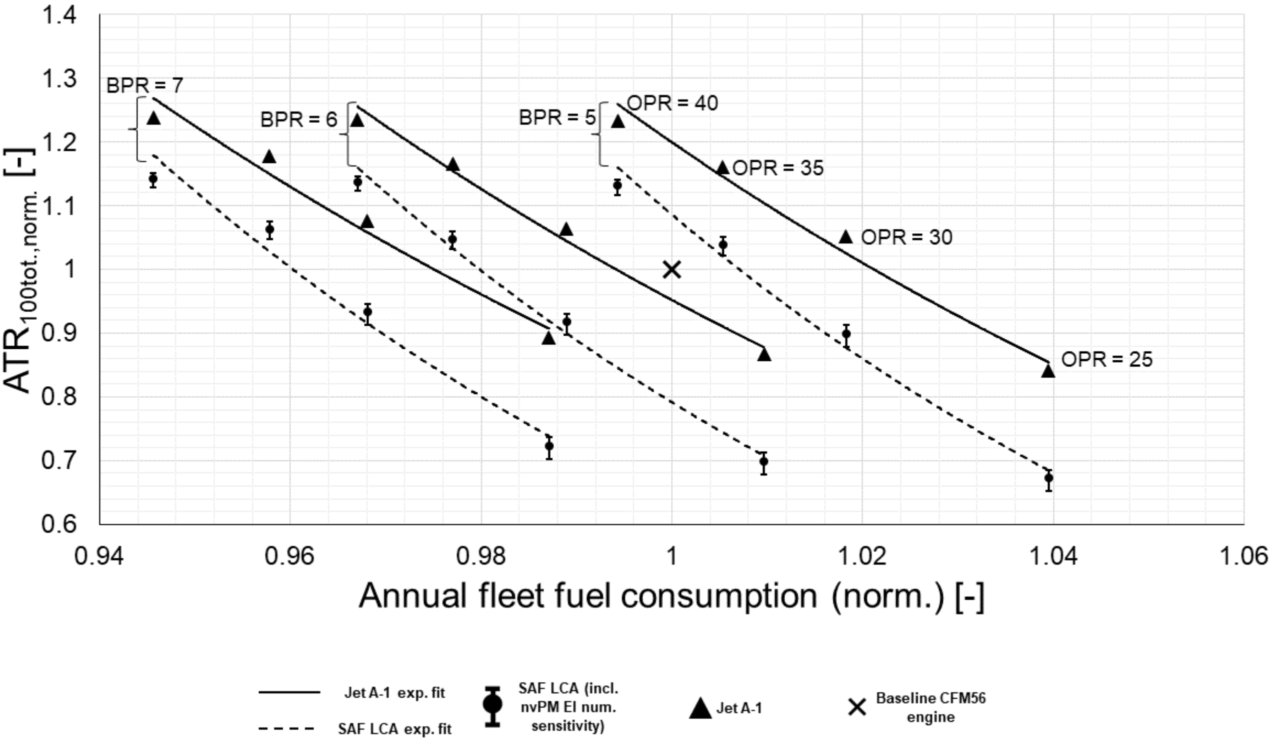

Figure 2: The comparison of the total ATR_{100} with fuel consumption for changing engine design. Both the parameters are normalized w.r.t.. the corresponding baseline values- represented in the figure in the middle (black cross)- as given in Table 1. The expected exponential-fitted curves for the two cases are shown, along with the sensitivity for the SAF case corresponding to different reductions in nvPM $EI_{num.cruise}$.

Compared to the baseline, the $ATR_{100,CO2}$ starts reducing from its initial value of 3.94% greater than the baseline, as the cycle pressure ratio increases, and goes lower than zero for OPR = 40, i.e. 0.56%, implying a smaller $ATR_{100,CO2}$ than baseline. Implementing SAF with its low $EICO_2$ than the baseline naturally gives a lower $ATR_{100,CO2}$. This is augmented by increasing cycle pressure ratios as fuel consumption is lowered, suggesting that SAF usage gives greater benefits at higher pressure ratios in terms of CO_2 climate impact. The $ATR_{100,CO2}$ due to SAF goes from 6.14% to 10.22% lower than the baseline $ATR_{100,CO2}$, as the OPR is increased. Irrespective of the fuel case in consideration, the reduction in the $ATR_{100,CO2}$ is roughly proportional to the reduction in the fuel consumption going from OPR = 25 to OPR = 40, i.e. close to 4.3%.

The $ATR_{100,contr.}$ for OPR = 25 is lower than the baseline, mainly due to lower temperatures than the baseline within the core, leading to less nvPM and thus, lower ice particles available for contrail formation. With an increasing pressure ratio, the conditions for nvPM formation become more favorable, ultimately leading to larger contrail effects for pressure ratios of 30 and above. The $ATR_{100,contr.}$ change w.r.t. pressure ratio is highly non-linear, as nvPM emissions, which act as contrail precursors, show a similar behavior w.r.t. changing combustion parameters, i.e. P_{t3} and T_{t3}. The application of SAF shows a lower $ATR_{100,contr.}$ than the corresponding Jet A-1 value due to the reduction in the nvPM emissions. For OPRs 25 and 30, the SAF application shows a lower $ATR_{100,contr.}$ than the baseline, but for the higher OPRs, even SAF application does not prevent a higher $ATR_{100,contr.}$ than the baseline. This is because at these pressure ratios, the nvPM numbers are high enough such that a 50% reduction would still result in a larger nvPM $EI_{num.cruise}$ than the baseline, ultimately leading to increased contrail effects than the baseline. A lower reduction in nvPM $EI_{num.cruise}$ of 45% from the baseline value causes the $ATR_{100,contr.}$ to increase by 3.01% at OPR = 25, and by 2.14% at OPR = 50, while a 53% reduction causes the $ATR_{100,contr.}$ to further reduce by 1.9% at OPR = 25, and by 1.45% at OPR = 50.

As far as the $ATR_{100,NOx}$ is concerned, with higher NO_x emissions due to higher cycle pressure ratios, the $ATR_{100,NOx}$ increases as well. This does not scale with NO_x emissions, unlike the case with CO_2 emissions. At high OPRs, the ATR_{100,NO_x} is higher, with almost a 40% increase compared to the baseline value for OPR = 40, the highest increase in any species' response for any pressure ratio. No change is observed for the SAF case.

Summing up the variations for all the species, for the Jet A-1 case, the total ATR_{100} is 15.94% lower than the baseline total ATR_{100} for OPR = 25, rising up to 23.21% for OPR = 40, also observed in Figure 2. SAF gives a larger reduction

DOI: 10.13009/EUCASS2023-318

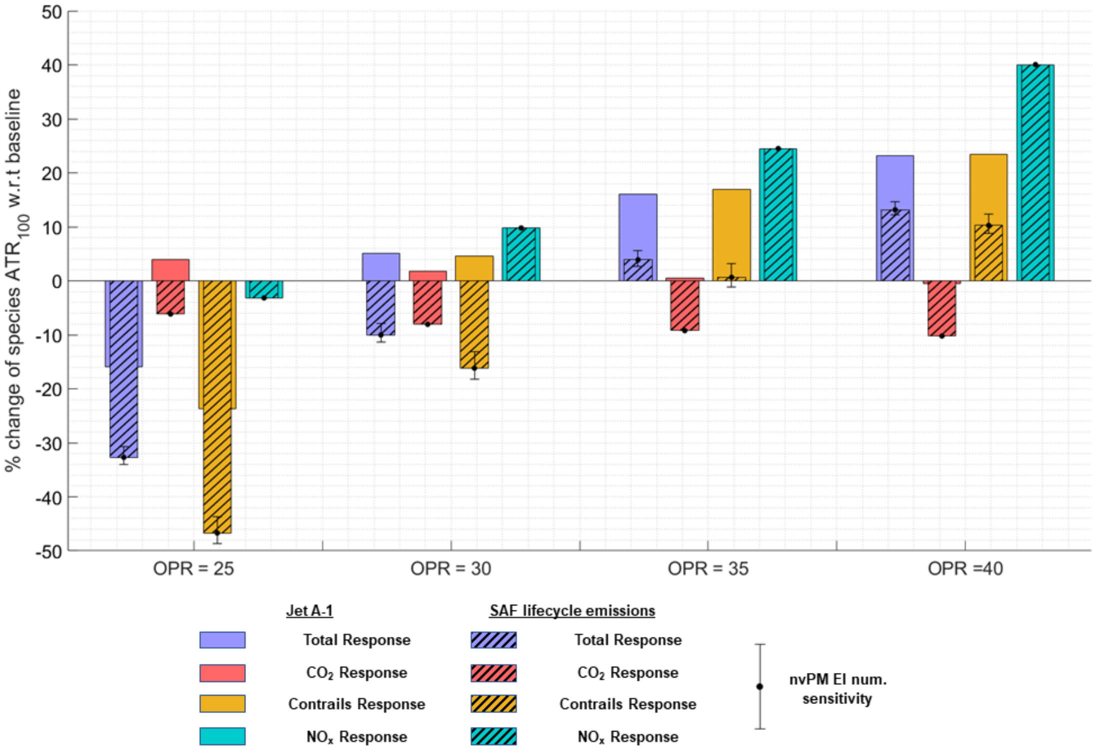

Figure 3: Comparison of the species ATR_{100} change w.r.t. their corresponding baseline configuration values in Table 2, with increasing OPR at a single BPR of 5. The changes in the total, CO_2 and NO_x responses are shown. The solid and hatched bars correspond to response changes in Jet A-1 and SAF lifecycle emissions cases respectively. The nvPM $EI_{num.}$ sensitivity is also shown.

of 32.71% in the total ATR_{100} at OPR = 25, which increases to 13.15% at OPR = 40 compared to the baseline configuration. The responses for the non-CO_2 species are more sensitive to changes in the engine design compared to the CO_2 response. This is mainly due to the well-mixed nature and the long lifetime of CO_2, which makes it roughly proportional to the reduction in fuel consumption. This also highlights the importance of non-CO_2 emissions from aviation and their impact on the climate. The limiting factor towards the total ATR_{100} is the $ATR_{100,contr.}$, as the $ATR_{100,contr}$ change across the pressure ratios results in an almost identical change in the total ATR_{100}.

A brief comparison of these observations are made for the other two BPR configurations, shown in Figure 4. The increase in the BPR reduces the fuel consumption of the fleet, which leads to a decrease in the CO_2 effects, even reducing the CO_2 effects lower than the baseline $ATR_{100,CO2}$ for some configurations. In contrast, due to increased core pressure and temperature during cruise at higher BPRs, the NO_x and nvPM emissions increase, leading to larger contrail and NO_x effects respectively. Since the non-CO_2 effects are more critical, the total ATR_{100} increases with increasing BPR. Considering the range of parameters in consideration, the BPR is found to be the less critical parameter than the OPR towards the climate impact, as the changes of the species' responses across BPR are much smaller compared to those across OPR.

4. Discussion

Through this research, we aimed to quantify the climate effects of general aviation-related species w.r.t. changing turbofan engine design. The focus was on analyzing the variation of these effects for a range of BPR and OPR values, particularly NO_x and contrails, as the two combined contribute more than two-thirds of the total ERF.[2] In addition, the impact of the lifecycle emissions of SAF HEFA with soy as the feedstock, on the climate effects of these species was also analyzed. There are ongoing efforts to reduce emissions from the aviation sector, however, assessing the climate effects of these emissions is necessary to make informed technology-related as well as policy-related decisions. In this context, this work can serve as a foundation for research related to the climate effects of civil aircraft engine design, and ultimately how these effects can be incorporated into the design of climate-friendly propulsion systems in the future.

DOI: 10.13009/EUCASS2023-318

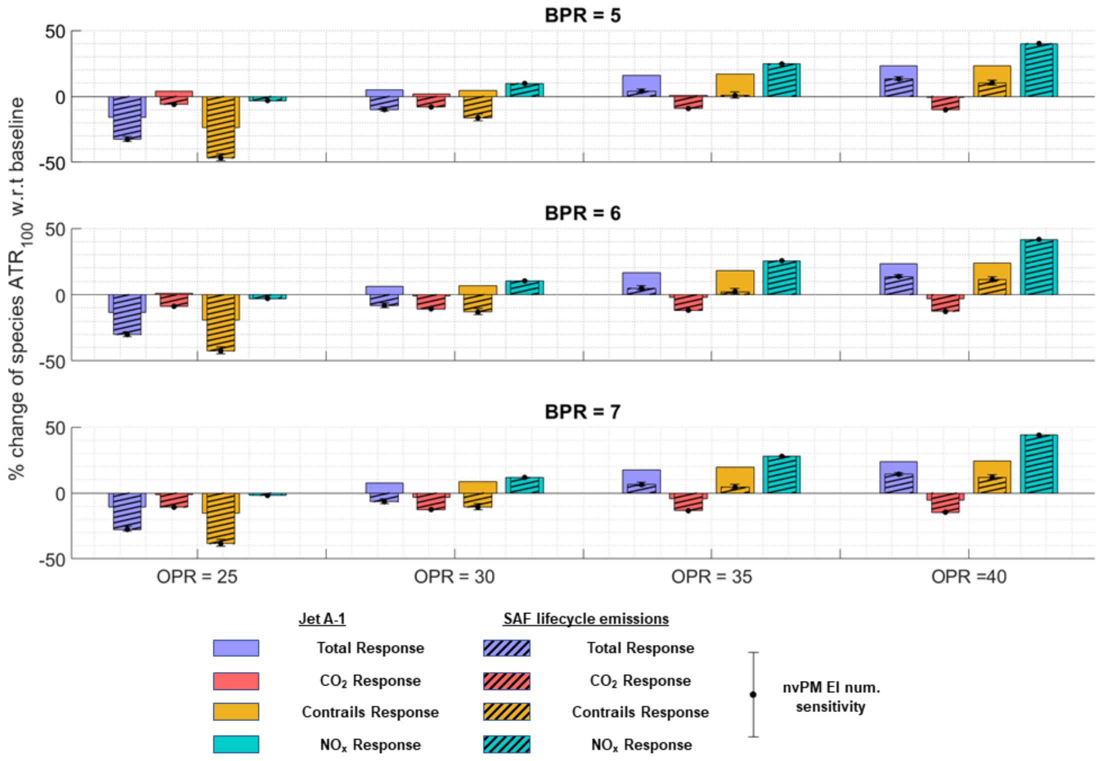

Figure 4: Comparison of the species ATR_{100} change w.r.t. their corresponding baseline configuration values, with increasing OPR at all BPRs. The changes in the total, CO_2 and NO_x responses are shown.

As the non-CO_2 emissions contribute much more towards the total temperature response, developing technologies that reduce these emissions will be critical towards reducing the climate impact of aviation. For instance, the implementation of lean combustion will enable large reductions in NO_x and nvPM emissions due to lower FAR, which can be used in synergy with increased OPR and BPR to reduce the climate effects of all the critical species. The methodology of this research enables a quantitative comparison of the climate effects of these options. In addition, the methodology can also be scaled or changed to generate higher-fidelity results, e.g. the application of CFD to analyze the formation of emissions, resulting in more accurate emission models/correlations. One key aspect related to modelling of aircraft/engine performance and climate impact evaluation is the related uncertainties and its quantification. These are statistical uncertainties, based on the model choices and the implemented approach. For instance, the $W_{app.payload}$ in section 2.1 can have uncertainties due to differences in the input weights as mission requirements change. Similarly, there are associated uncertainties with the lifetime, RF and the climate sensitivity parameter (i.e. the factor that translates RF to ATR_{100}). Dahlmann et al. (2016)[8] in their research have described a methodology to reliably assess climate mitigation options taking into account the climate effects uncertainties. This methodology, where only atmospheric uncertainties are considered, can be extended to the current research, encompassing the uncertainties related to other elements such as aircraft/performance or emission predictions. While this will produce more robust results, it is out of the scope of this study. Further, only a tiny subset of the global aviation network is analyzed, with the climate simulations and responses pertaining to only this subset. It is expected that transitioning to a global aviation coverage consisting of different aircraft, along with considering detailed scenarios with reasonable predictions about the future of aviation will result in a more accurate and realistic climate analysis.

5. Conclusions

Following the general trend within the engine design framework, increasing the pressure ratio and bypass ratio of the CFM56 engine at a similar combustion technology level for a subset of the global A320 traffic improves fuel consumption, but leads to a higher climate impact, due to higher non-CO_2 effects. For a particular reduction in fuel consumption, the increase in the climate impact is much larger. This is mainly driven by the non-CO_2 emissions of NO_x and contrails, and their respective effects, which together contribute upwards of 80% of the total effects for the

DOI: 10.13009/EUCASS2023-318

selected fleet and background aviation scenario. The variation of these effects w.r.t. engine design parameters is highly non-linear. Out of the two, contrail-related effects are found to be the driving factor behind the total response change w.r.t. changing pressure ratio and bypass ratio for the chosen conditions of this research. SAF plays a critical role in reducing the total aviation effects by virtue of a reduction in net CO_2 and contrail-related effects, with a greater reduction potential for a high-pressure ratio engine.

6. Acknowledgement

This research has been carried out as part of a Dutch Research Council (NWO) supported project (Fly Green: Choices at Crossroads, Project 17367). The authors would like to thank Prof. Dr. Volker Grewe from the Deutsches Zentrum für Luft- und Raumfahrt (DLR), Institut für Physik der Atmosphäre, Oberpfaffenhofen and Chair for Climate Effects of Aviation, Aerospace Engineering, Delft University of Technology for providing access to the AirClim model used in this research.

Nomenclature

ATR	Average Temperature Response
BPR	Bypass ratio
CCM	Climate chemistry Model
CORSIA	Carbon Offsetting and Reduction Scheme for International Aviation
EI	Emission Index
ERF	Effective Radiative Forcing
FAR	Fuel-to-Air ratio
FPR	Fan pressure Ratio
GHG	Greenhouse gas
GSP	Gas Turbine Simulation program
HEFA	Hydrotreated Esters and fatty acids
ICAO	International Civil Aviation Organization
ILUC	Induced land-use change
IPCC	Intergovernmental Panel for Climate Change
ISSR	Ice Supersaturated region
LCA	Life Cycle Assessment
LHV	Lower Heating value
LTO	Landing and Takeoff cycle
nvPM	non-volatile Particulate Matter
OEW	Operating Empty Weight
OPR	Operating Pressure Ratio
PMO	Primary- Mode Ozone
RF	Radiative Forcing
SAF	Sustainable Aviation Fuel
SLS	Static Sea Level
SSP	SocioEconomic Pathways
TIT	Turbine Inlet Temperature
TSFC	Thrust Specific fuel consumption

References

[1] Valérie Masson-Delmotte, Panmao Zhai, Anna Pirani, Sarah L Connors, Clotilde Péan, Sophie Berger, Nada Caud, Y Chen, L Goldfarb, MI Gomis, et al. Climate change 2021: the physical science basis. *Contribution of working group I to the sixth assessment report of the intergovernmental panel on climate change*, 2, 2021.

[2] David S Lee, David W Fahey, Agnieszka Skowron, Myles R Allen, Ulrike Burkhardt, Qi Chen, Sarah J Doherty, Sarah Freeman, Piers M Forster, Jan Fuglestvedt, et al. The contribution of global aviation to anthropogenic climate forcing for 2000 to 2018. *Atmospheric Environment*, 244:117834, 2021.

DOI: 10.13009/EUCASS2023-318

[3] Herbert Appleman. The formation of exhaust condensation trails by jet aircraft. *Bulletin of the American Meteorological Society*, 34(1):14–20, 1953.

[4] Ernst Schmidt. Die unstrung von eisnebel aus den auspuffgasen von flugmotoren. *Schriften der Deutschen Akademie der Luftfahrtforschung, Verlag R. Oldenbourg, München, Heft 44*, 5(44):1–15, 1941.

[5] Christiane Voigt, Jonas Kleine, Daniel Sauer, Richard H Moore, Tiziana Bräuer, Patrick Le Clercq, Stefan Kaufmann, Monika Scheibe, Tina Jurkat-Witschas, Manfred Aigner, et al. Cleaner burning aviation fuels can reduce contrail cloudiness. *Communications Earth & Environment*, 2(1):114, 2021.

[6] W. P. J. Visser. Generic analysis methods for gas turbine engine performance: The development of the gas turbine simulation program gsp. 2015.

[7] V. Grewe and A. Stenke. Airclim: an efficient tool for climate evaluation of aircraft technology. *Atmospheric Chemistry & Physics*, 8(16), 2008.

[8] K. Dahlmann, V. Grewe, C. FrÃ¶mming, and U. Burkhardt. Can we reliably assess climate mitigation options for air traffic scenarios despite large uncertainties in atmospheric processes? *Transportation Research Part D: Transport and Environment*, 46:40–55, 2016.

[9] WPJ Visser and MJ Broomhead. Gsp user manual. *National Aerospace Laboratory NLR, Amsterdam, the Netherlands, NLR TR-99410*, 2000.

[10] PD Norman, DH Lister, M Lecht, P Madden, K Park, O Penanhoat, C Plaisance, and K Renger. Development of the technical basis for a new emissions parameter covering the whole aircraft operation: Nepair. *European Commission, Final TR G4RD-CT-2000-00182, Brussels, Belgium*, 2003.

[11] ICAO. Icao annex 16: Environmental protection, volume ii–aircraft engine emissions, 2008.

[12] Volker Grewe, Arvind Gangoli Rao, Tomas Grönstedt, Carlos Xisto, Florian Linke, Joris Melkert, Jan Middel, Barbara Ohlenforst, Simon Blakey, Simon Christie, et al. Evaluating the climate impact of aviation emission scenarios towards the paris agreement including covid-19 effects. *Nature Communications*, 12(1):3841, 2021.

[13] Lukas Durdina, Benjamin T Brem, Ari Setyan, Frithjof Siegerist, Theo Rindlisbacher, and Jing Wang. Assessment of particle pollution from jetliners: from smoke visibility to nanoparticle counting. *Environmental Science & Technology*, 51(6):3534–3541, 2017.

[14] Brian C OâNeill, Elmar Kriegler, Kristie L Ebi, Eric Kemp-Benedict, Keywan Riahi, Dale S Rothman, Bas J Van Ruijven, Detlef P Van Vuuren, Joern Birkmann, Kasper Kok, et al. The roads ahead: Narratives for shared socioeconomic pathways describing world futures in the 21st century. *Global environmental change*, 42:169–180, 2017.

[15] David S Lee, Giovanni Pitari, Volker Grewe, K Gierens, Joyce E Penner, Andreas Petzold, MJ Prather, Ulrich Schumann, A Bais, T Berntsen, et al. Transport impacts on atmosphere and climate: Aviation. *Atmospheric environment*, 44(37):4678–4734, 2010.